ELSEVIER

Journal of Magnetism and Magnetic Materials 169 (1997) 253–260

Journal of magnetism and magnetic materials

Canted antiferomagnetic structure of the novel compound Er_3Ge_4 by neutron diffraction and magnetic measurements

P. Schobinger-Papamantellos[a,*], O. Oleksyn[a,1], C. Ritter[b], C.H. de Groot[c], K.H.J. Buschow[c]

[a] *Laboratorium für Kristallographie, ETHZ, CH-8092 Zürich, Switzerland*
[b] *Institut Laue-Langevin, 156X, 38042 Grenoble Cédex, France*
[c] *Van der Waals-Zeeman Institute, University of Amsterdam, 1018 XE Amsterdam, The Netherlands*

Received 23 September 1996; revised 6 December 1996

Abstract

The magnetic ordering of the novel orthorhombic compound Er_3Ge_4 (Cmcm) with two Er sites has been studied by neutron diffraction and magnetic measurements. Er_3Ge_4 orders antiferromagnetically below $T_N = 7.3$ K. The magnetic moments of the Er_1 atoms (at 8(f)) make an angle of 35.5(3)° with the y-axis while the moments of the Er_2 atoms (at 4(a)) are perpendicular to it within the $(0, y, z)$ plane. This triangular antiferromagnetic moment arrangement of the two sublattices in the plane $(0, y, z)$ relates to the stacking of the rare earth triangular prism slabs along the a axis. Adjacent prisms along b or c are shifted by $x = \frac{1}{2}$ and display different chiralities. The 1.5 K ordered magnetic moment values of Er_1 and Er_2 are 7.32(5) μ_B/Er and 6.37(6) μ_B/Er, respectively. The two Er sublattices order simultaneously but display a completely different thermal behaviour indicating the existence of competing interactions. The magnetic space group $C_P\ (\frac{2}{m}\frac{2'}{c}\frac{2_1'}{m})\ (Sh_{57}^{391})$ has a primitive lattice associated with the wave vector $q = (0\ 1\ 0)$.

PACS: 74.25.Ha; 75.20.En; 75.25. + z; 75.30.-m; 75.50.Ee; 76.30.Kg

Keywords: Rare earth; Crystal structure; Magnetic structure; Neutron diffraction

1. Introduction

Rare earth silicides and germanides have been known for some time [1–3] and have attracted the interest of several investigators because of their manifold structures and magnetic properties [4]. Eremenko who has systematically investigated

* Corresponding author. E-mail: nelly@kristall.erdw.ethz.ch; fax: + 41-1-632-1133.

[1] On leave from the Institute of Inorganic Chemistry, Lviv State University, Lviv, Ukraine.

PII S0304-8853(96)00750-0

[3, 4] the R-Ge and R-Si (R = rare-earth) binary phase diagrams reports the existence of a novel type of compounds at about 58% Ge/Si (R_3Ge_4, R_3Si_4).

Recent neutron and magnetic studies [5, 6] have shown that the majority of the R_3Si_4 compounds are deficient in Si and that all of them crystallise in a novel type of structure related to the CrB and a-$GdSi_2$ structure types. The vacancies are distributed selectively on one of the Si sites which is up to about 50% unoccupied leading to the composition $R_2Si_{3-\delta}$. The structure is orthorhombic and comprises two R sites and three silicon sites. The magnetic ordering of these compounds is interesting because of the existence of competing intrasite I_{AA}, I_{BB}, and intersite I_{AB} interactions which lead to complex ordering phenomena. In the ferromagnetic compounds of the light rare earths the intersite interaction I_{AB} is weak and the two rare earth sites display a completely different magnetic behaviour leading to a two step magnetic ordering for the sublattices [5a, 5c, 5d, 5e]. Selective replacement of one of the Pr atoms by nonmagnetic Y leads to a break down of ferromagnetism in $Pr_2Si_{3-\delta}$.

For the antiferromagnetic stoichiometric $Tb_2Si_{3-\delta}$ ($\delta = 0$) compound the intrasite interaction I_{AB} is dominant and leads to the same ordering temperature for both sublattices. The magnetic moment arrangement corresponds to a three-dimensional canted structure comprising six Tb sublattices. There is a strong difference in the orientations and magnitude of the Tb moments between the two Tb sites (7.26 μ_B/Tb_1 and 1.29 μ_B/Tb_2).

Contrary to the silicon compounds of nominal composition R_3Si_4, the R_3Ge_4 (R = Dy, Ho, Er) were found to be stoichiometric [6] and to crystallise with a novel orthorhombic structure type (Cmcm space group) with two rare earth sites and three germanium sites.

The structure determination of Er_3Ge_4 and the isomorphic R_3Ge_4 compounds (R = Tb, Dy, Ho, Er, Tm), was based on X-ray powder data. In the present investigation we will report on the magnetic properties and magnetic ordering of the Er_3Ge_4 compound based on magnetic measurements and neutron diffraction.

2. Sample preparation

The polycrystalline sample of composition Er_3Ge_4 was prepared by arc melting of the elements in an atmosphere of purified argon gas. The purity of the starting materials was 99.9% for Er and 99.99% for Ge. After arc melting the sample was vacuum annealed at the temperature range 800°C for three weeks and subsequently quenched in water. The purity of the sample was examined by X-ray powder diffraction.

3. Magnetic measurements

Magnetic measurements were made with a SQUID magnetometer. The temperature dependence of the magnetisation measured in a field of 0.1 T (see Fig. 1a) shows that Er_3Ge_4 orders antiferromagnetically at about $T_N = 7.3$ K. From the field dependence of the moment at 5 K it is derived that the antiferromagnetic structure is broken easily, starting already below 0.5 T. No moment saturation is found, however, for the highest field strength applied. This can be taken as indicative of a substantial magnetic anisotropy present in this compound.

4. Neutron diffraction

Neutron diffraction experiments were carried out at the facilities of the ILL reactor (Grenoble) D1B diffractometer ($\lambda = 2.52$ Å). The data were collected in the temperature range 1.5–20 K with an increment of 0.5 K, cf. Fig. 2. The step increment in 2θ was 0.2°. The data analysis was performed by the Fullprof program [7].

4.1. Nuclear structure

The refined neutron patterns in the paramagnetic state confirm the structure and parameters reported [6]. Results are displayed in Fig. 3 (top part) and in Table 1.

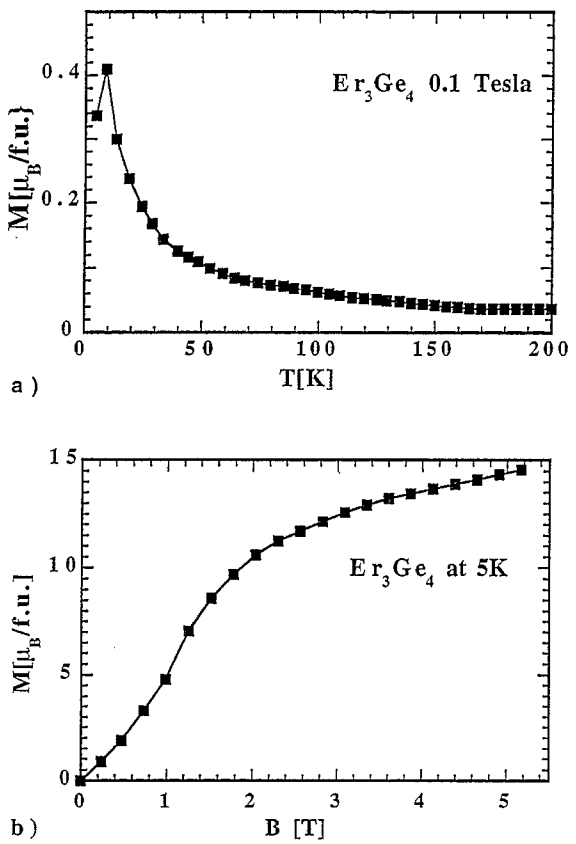

Fig. 1. (a) Temperature dependence of the magnetic moment of Er_3Ge_4 in a field of 0.1 T. (b) Field dependence of the magnetic moment of Er_3Ge_4 at 5 K.

4.2. Magnetic structure

In Figs. 2 and 3 one observes several strong magnetic lines in the low 2θ region and at reciprocal lattice positions that do not obey the C-lattice reflection conditions. The wave vector is $\boldsymbol{q} = (0, 1, 0)$ which corresponds to the anticentered magnetic C_P lattice. Magnetic order sets in below $T_N = 7.3$ K and maintains the same peak topology over the whole magnetically ordered regime. There are eight magnetic space groups associated with the Cmcm space group and the wave vector $\boldsymbol{q} = (0, 1, 0)$ (magnetic C_P lattice) [8–10].

The possible magnetic modes of the 8(f) and 4(c) Wyckoff positions occupied by the two Er atoms are displayed in Table 2. The 4(c) special site may have only a uniaxial type of ordering with either an A(+ − − +) or C(+ + − −) mode. The 8(f) site may have also a two -dimensional ordering. The refinement of the magnetic intensities leads to a collinear arrangement of the Er_2 magnetic moments along the $\boldsymbol{c}$ axis with opposite signs for the atoms (1) $(0, y, z)$ and (2) $(0, -y, \frac{1}{2} + z)$ related by the i or $(2_x, 2_y, 2_{1z})$ operations. Taking into consideration the C_P antitranslation operation one obtains the mode $A_z(+ - - +)$. The Er_1 (8(f) site) has the modes C_y–C_y and G_z–G_z in the notation of Ref. [8]. This arrangement remains invariant under the transformations of the magnetic space group $C_P\left(\frac{2\ 2'\ 2_1'}{m'\ c\ m}\right)$ (Sh_{57}^{391}). The good agreement between the experimental and the calculated pattern (Fig. 3) and the low values of the reliability factors $R_n = 4.46\%$, $R_m = 2.57\%$, $R_{wp} = 6.98\%$, $R_{exp} = 2.6\%$ (see Table 1) lends credence to the correctness of the model proposed.

At 1.5 K the ordered moment values of the Er_1 and Er_2 sites are 7.32(5) μ_B/Er and 6.37(6) μ_B/Er, respectively. These values are lower than the free-ion value of Er^{3+} ($gJ\mu_B = 9\ \mu_B$) which is most probably due to crystal field effects. We mentioned already that the lack of saturation of the magnetic moment for field strength much higher than the metamagnetic transition can be interpreted as magnetic anisotropy present in Er_3Ge_4. A large magnetocrystalline anisotropy would be in agreement with the crystal-field induced moment reduction mentioned above. However, the magnetic structure determination offers another possibility for the field dependence of the moment shown in Fig. 1b. It is possible that the metamagnetic transition applies only to one of the Er sites, leaving the other Er sublattice antiferromagnetic. We will return to this possibility later on in the text.

As can be seen in the projection along the shortest lattice period $\boldsymbol{a}$ (Fig. 4) the magnetic structure consists of four slabs of triangular prisms along $\boldsymbol{a}$ which are composed by two Er_1 and one Er_2 atoms. The moment angle between the two Er_1 atoms is 110° and the angle between the Er_1 and Er_2 atoms is 125°. The average value of 117.5° within the error limit is suggestive of a regular triangle. We can label the four isolated prisms by the same number as the Er_2 atom (dark colour) they contain. The structure is then very easily described in the following way: The triangular

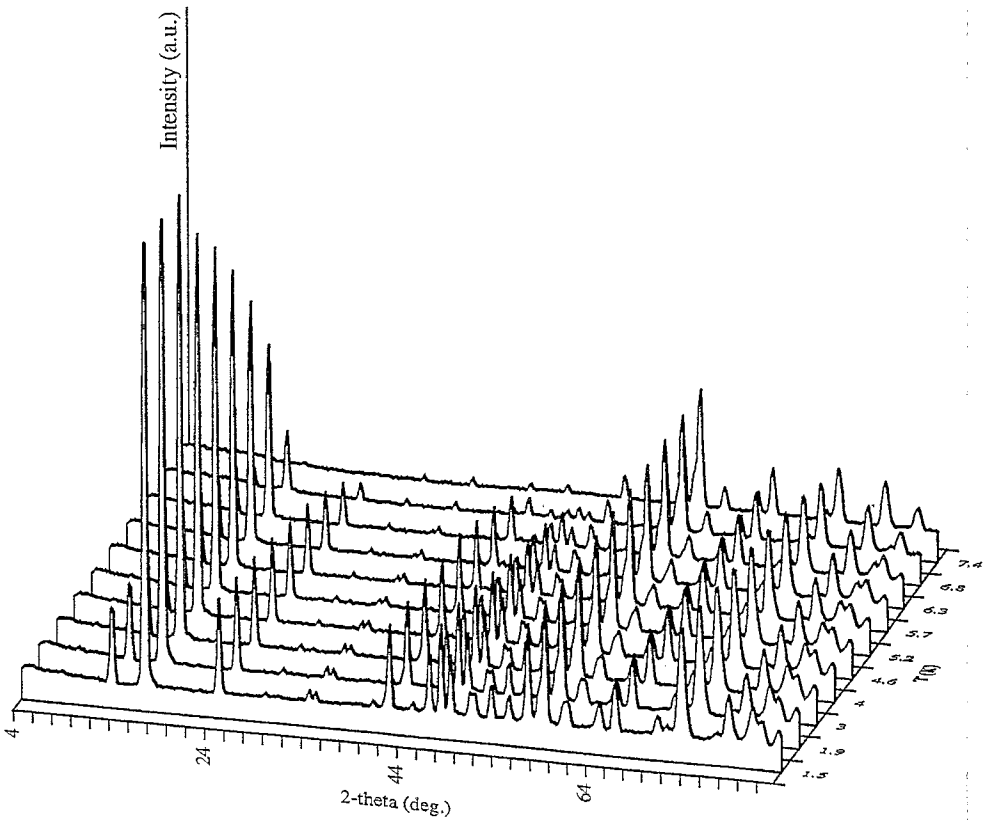

Fig. 2. A perspective view of the onset of magnetic order in Er_3Ge_4. Neutron patterns collected with the D1B spectometer for $T \leqslant T_N = 7.3$ K and for $4° < 2\theta < 83.8°$.

moment arrangement of prism 1 with origin at $x = 0$ corresponds to a right screw. Prisms 1 and 3 related by the anticentering C_P operation have opposite chiralities. Prism 2 related by the centring operation to prism 1 maintains the same chirality while prism 4 (at $x = \frac{1}{2}$) obtained by the action of the screw axis 2_{1z} at $(\frac{1}{4}, \frac{1}{4}, 0)$ changes its chirality. So the total consists of four triangular prisms with a two dimensional canted moment arrangement two of them with right ($x = 0$) and two with left chiralities ($x = \frac{1}{2}$) corresponding to six Er sublattices.

4.3. Thermal evolution of magnetic order

Fig. 5 shows the thermal evolution of some selected magnetic integrated intensities. The used I_{obs} values are extracted from the observed data by profile analysis of the entire patterns at all temperatures. The intensity of the $\{1\ 0\ 2\}$ reflection is seen in Fig. 5 (top part) to display a smooth increase with decreasing temperature while the intensity of the (0 3 0) reflection rises with a less steep slope and shows a discontinuity and a steeper slope below 4.0 K. The structure factors of the (0 3 0) and $\{1\ 0\ 2\}$ reflections comprise single contributions arising from the μ_{Er2z} and μ_{Er1y} moment components, respectively.

The structure factors of the (0 1 0) and $\{0\ 1\ 2\}$ reflections shown in the bottom part of Fig. 5, comprise μ_z contributions of both Er sites, and contributions of all components, respectively. The intensity change of the (0 1 0) reflection shows a steep increase in the high temperature region and a slope change at about 4.0 K. This is related to the opposite sign of the μ_z components of the two Er sites in the magnetic structure factor $F(0\ 1\ 0) = (4 \times$

$0.327\mu_{Er2z} + 8 \times 0.867\mu_{Er1z}$). In contrast, the thermal evolution of the {0 1 2} reflection shows no anomaly as all components add up.

The thermal behaviour of the magnetic intensities suggests different behaviours of the Er_1 and Er_2 sublattices occupying the 8(f) and 4(c) crystallographic sites, respectively (see Fig. 6). The two sublattices order at the same T_N but they have different preferred directions of antiferromagnetism and different thermal evolution. The ordering of the Er_1 sublattice is predominant in the high temperature region and displays a steeper increase than that of Er_2 the latter being closer to a linear evolution with a small anomaly below ≈ 4 K. The moments of the Er_2 site are confined to the *c* direction while the moments of Er_1 are at high temperatures closer to the ***b*** axis. The angle ϕ_b between the moment direction of the Er_1 atom and ***b*** direction is 31° and is *T*-dependent. Just below $T_N = 7.3$ K it is 31°, between 4 and 5.8 K it has the value of 34.4°. At 4.0 K the moments turn to 35.4°.

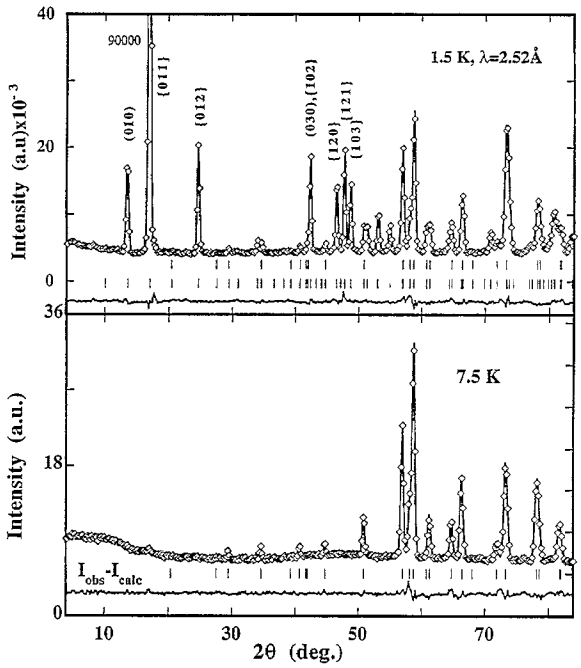

Fig. 3. Observed, calculated and difference neutron diagram of Er_3Ge_4 measured (a) in the paramagnetic state (bottom part) and (b) in the magnetically ordered state at 1.5 K (top part).

The change in slope of the Er_2 moment *T* dependence at $T \approx 4$ K is tidely connected with the increase of the ϕ_b angle of sublattice Er_1 with the ***b*** axis (see Fig. 6). This can be explained as a field action on a triangular canted moment arrangement (see inset Fig. 4) [11]. The field direction is defined by the moment direction of sublattice Er_2 which points along *c*. This field direction is opposite to the line bisecting the Er_1–Er_1 angle ($\phi_1 > 110°$ at high temperatures). Due to the strong antiferromagnetic interaction I_{12} between the two sublattices any increase of moment Er_2 will force the Er_1 moments to turn in the opposite direction. As the Er_1–Er_1 angle becomes smaller $<110°$ the angle $\phi_b = (\frac{1}{2}\pi - \phi_1)$ becomes larger as observed in Fig. 6.

Table 1
Refined parameters from neutron data of Er_3Ge_4 (space group Cmcm: (a) at 7.4 K (paramagnetic state) and (b) at 1.5 K in the magnetically ordered state (magnetic space group C_P ($\frac{2}{m}\frac{2'}{c}\frac{2_1'}{m}$) ($Sh_{57}^{391}$)

Temperature	7.5 K		1.5 K	
Atom	*y*	*z*	*y*	*z*
Er_1 at 8f: (0, *y*, *z*)	0.333(1)	0.096(1)	0.3323(8)	0.0970(4)
Er_2 at 4c: (0, *y*, $\frac{1}{4}$)	0.053(2)	0.25	0.0484(7)	0.25
Ge_1 8f: (0, *y*, *z*)	0.377(1)	0.8880(6)	0.379(1)	0.890(1)
Ge_2 at 4c: (0, *y*, $\frac{1}{4}$)	0.778(1)	0.25	0.779(1)	0.25
Ge_3 at 4a: (0, 0, 0)	0.0	0.0	0.0	0.765(4)
Er_1: μ_{xyz} [μ_B]			5.96(5)	4.25(3)
μ_T [μ_B], ϕ_b (°)			7.32(5)	35.5(2)
Er_2: μ_{xyz}[μ_B]				− 6.37(8)
a (Å), *b* (Å), *c* (Å)	3.9878(7), 10.509(2), 14.079(3)		3.9883(4), 10.513(1), 14.083(1)	
R_n (%), R_m (%)	4.69, —		4.46, 2.57	
R_{wp} (%), R_{exp} (%)	9.4, 4.89		6.98, 2.61	

Table 2
Magnetic space groups of the Cmcm space group associated with the wave vector $\boldsymbol{q} = (0\ 1\ 0)$ (C_P lattice, found in R_3Ge_4 compounds). Indicated are also the corresponding magnetic modes F(+ + + +), G(+ − + −), C(+ + − −) and A(+ − − +) of the R sites at 4(c) and 8(f)

		$C_P \frac{2\ 2\ 2_1}{m\ c\ m}$ i	$C_P \frac{2\ 2'\ 2_1'}{m'\ c\ m}$ i'	$C_P \frac{2'\ 2\ 2_1'}{m\ c'\ m}$ i'	$C_P \frac{2'\ 2'\ 2_1}{m\ c\ m'}$ i	$C_P \frac{2'\ 2'\ 2_1}{m'\ c'\ m}$ i	$C_P \frac{2\ 2'\ 2_1'}{m\ c'\ m'}$ i	$C_P \frac{2'\ 2\ 2_1'}{m'\ c\ m'}$ i	$C_P \frac{2\ 2\ 2_1}{m'\ c'\ m'}$ i'
		Sh_{51}^{301}	Sh_{57}^{391}	Sh_{59}^{414}	Sh_{62}^{453}	Sh_{62}^{454}	Sh_{58}^{402}	Sh_{60}^{431}	Sh_{52}^{318}
R_2 at 4(c)	Gen el	x y z	x y z	x y z	x y z	x y z	x y z	x y z	x y z
$xyz + C_P$			A		A	C	C	C	A
1. $0, y, \frac{1}{4}$	e		+		+	+	+	+	+
2. $0\ -y, \frac{3}{4}$	i		−		−	+	+	+	−
R_1 at 8(f)									
$xyz + C_P$		A-A	C-C G-G	C-C	G-G	A-A F-F	F-F	F-F A-A	G-G C-C
1. $0, y, z$	e h_1	+	+ +	+	+	+ +	+	+ +	+ +
2. $-0\ -y, z+\frac{1}{2}$	2_{1z} h4	−	+ −	+	−	− +	+	+ −	− +
3. $0, y, -z+\frac{1}{2}$	2_y h3	−	− +	−	+	− +	+	+ −	+ −
4. $0, -y, -z$	2_x h2	+	− −	−	−	+ +	+	+ +	− −

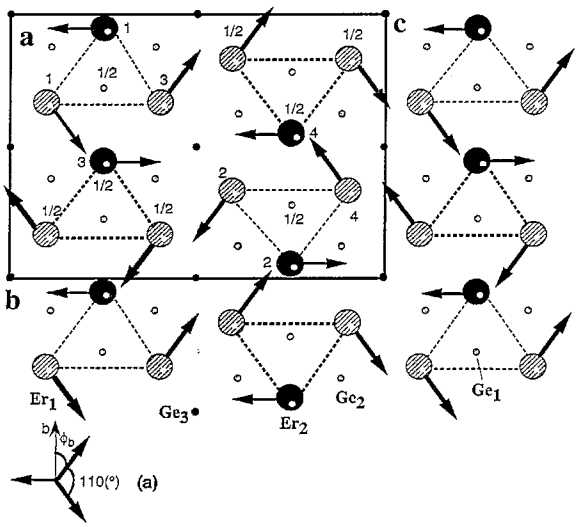

Fig. 4. Schematic representation of the triangular moment arrangement in Er_3Ge_4 when viewed along the [1 0 0] direction. The inset (a) shows the intersublattice angles.

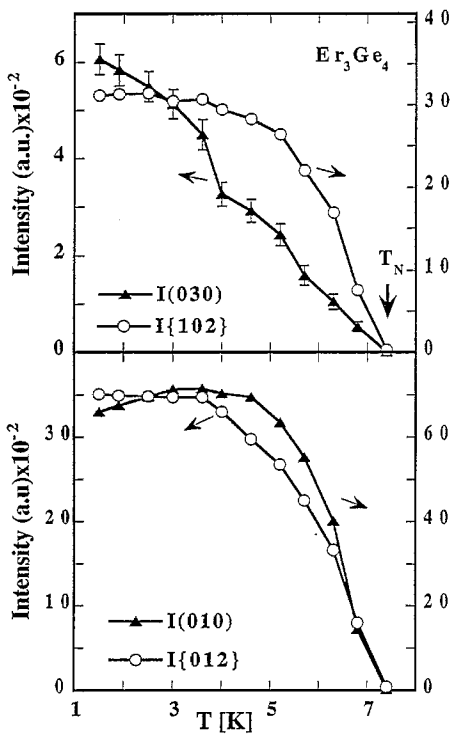

Fig. 5. Temperature dependence of the magnetic intensity of various reflections of Er_3Ge_4: peaks associated with a single contribution (0 3 0) with μ_{Er2z} and {1 0 2} with μ_{Er1y} (top part); peaks with more than one contributions (0 1 0) with all μ_z and {0 1 2} with all contributions.

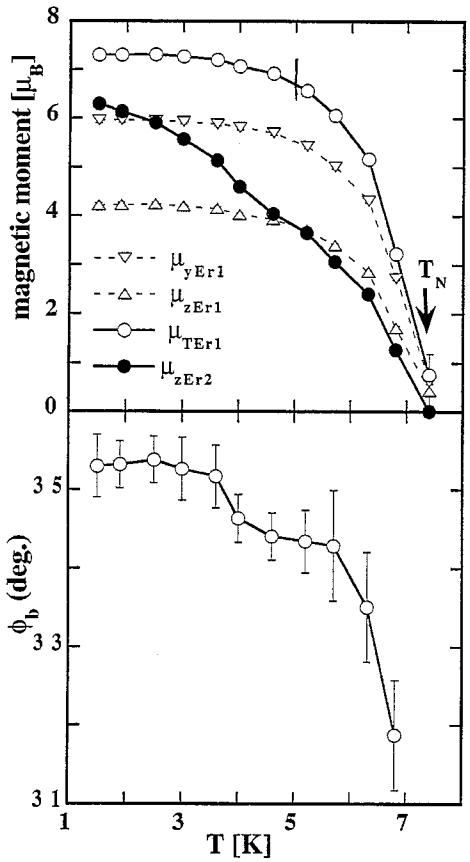

Fig. 6. Temperature dependence of: the magnetic moment components of the Er_1 (8(f)) and Er_2 (4(c)) sites (top part); the angle ϕ_b between the Er_1 magnetic moment and the b direction in Er_3Ge_4 (bottom part).

5. Conclusions

The existence of the novel phase Er_3Ge_4 reported in Ref. [6] has been confirmed. The two crystallographically distinct magnetic Er sites form a two dimensional canted antiferromagnetic triangular structure below $T_N = 7.3$ K. The moments of the two Er sites have different values and different preferred orientations of antiferromagnetism. The intersite interaction I_{12} is important over the entire ordered region since the sublattices Er_1 and Er_2 order at the same temperature and their different thermal behaviour displays anomalies at the same temperatures.

Furthermore, the results shown in Fig. 6 suggest that the Er_1 intrasublattice interaction I_{11} is the most important one and that the Er_2 intrasublattice interaction I_{22} is the weakest one. The shortest separation between the Er_1 and Er_2 atoms corresponds to the two corresponding sides of each of the triangles shown in Fig. 4. Apparently it is the antiferromagnetic nature of the intersublattice interaction I_{12} that causes frustration of the Er_1 moment ordering and leads to the canted moment arrangement of the Er_1 lattice.

If one uses the relative strengths of I_{11}, I_{12} and I_{22} for interpreting the field dependence of the magnetisation at 5 K shown in Fig. 1b, the following picture emerges: Because I_{22} is the smallest interaction the antiferromagnetism of the Er_2 lattice will be broken first and lead to a metamagnetic transition in which the Er_2 moments are aligned ferromagnetically in the c direction. In view of the strong antiferromagnetic intersublattice coupling I_{12} this will lead to a field-stabilized magnetic structure in which the triangular moment arrangement in the two types of prisms (Fig. 4) now have the same chirality. The net moment associated with this magnetic structure would be equal to $\mu_{zEr1} - 2\mu_{zEr2}$. By interpolation of the data plotted in Fig. 6 one can derive values for μ_{zEr1} and μ_{zEr2}, both being equal to 4 μ_B at 5 K. The net moment of the initial field stabilized structure would then be equal to $2 \times 4\ \mu_B - 4\ \mu_B = 4\ \mu_B$.

Most likely the net moment becomes substantially larger because it can be expected that the applied field leads to some enhancement of the individual Er moment values, and because the field will bend the canted Er_1 moments into the parallel direction. In the latter case, when the canting of the Er_1 moments would have completely disappeared, the field-stabilized magnetic structure consists of mutually parallel Er_2 moments oriented antiparallel to mutually parallel Er_1 sublattice moments. The corresponding net magnetic moment at 5 K, using again the data displayed in Fig. 6, would then be equal to $2 \times 6.8\ \mu_B - 4\ \mu_B = 9.6\ \mu_B$. This value is in reasonable agreement with the moment found after the metamagnetic transition in Fig. 1b. Further increase of the applied field would cause the antiparallel Er_2 and Er_1 sublattice moments to bend towards each other until they have ultimately become parallel.

However, in view of the complexity of the underlying magnetic structure, it is difficult to predict how this structure actually develops with increasing field strength. One of the main difficulties is that one does not know in how far the zero-field triangular magnetic structure as observed by neutron diffraction is controlled by different crystal field interactions at the two rare earth sites, possibly leading to different preferred moment directions at these two sites. Anyhow, for complete parallel arrangement of all moments at 5 K one would derive from Fig. 6 a value of at least 17.4 μ_B. As can be seen in Fig. 1b, this value has not yet been reached in the maximum field strength applied.

Acknowledgements

This work is financially supported by the Swiss National Foundation, Bern.

References

[1] A. Iandelli and A. Palenzona, in: Handbook on the Physics and Chemistry of Rare-Earths, Vol. 2, Eds. K.A. Gschneidner, Jr. and L. Eyring (North-Holland, Amsterdam, 1979) p. 1.
[2] P. Rogl, in: Handbook on the Physics and Chemistry of Rare Earth Metals, Vol. 7, Eds. K.A. Gschneidner, Jr. and L. Eyring (North-Holland, Amsterdam, 1984).
[3] M. Eremenko and I.M. Obushenko, Sov. Powder Metall. Met. Ceram. 19 (1980) 482.
[4] P. Villars, Pearsons Handbook of Crystallographic Data for Intermetallic Phases, Eds. P. Villars and L.D. Calvart, 2nd ed. (ASM International, Materials Park, OH, 1991); Handbook of Ternary Alloy Phase Diagrams (ASM International, Materials Park, OH, 1995).
[5] P. Schobinger Papamantellos, D.B. de Mooij, K.H.J. Buschow, P. Fischer: (a) J. Alloys Compounds 178 (1992) 151; (b) J. Magn. Magn. Mater. 119 (1993) 69; (c) J. Magn. Magn. Mater. 114 (1992) 131; (d) J. Alloys Compounds 185 (1992) L5; (e) J. Alloys Compounds 198 (1993) 47.
[6] O.Ya. Oleksyn and O.I. Bodak, J. Alloys Compounds 210 (1994) 19.
[7] J. Rodriguez-Carvajal, Physica B 192 (1993) 55.
[8] E.F. Bertaut, in: (a) Magnetism, Eds. G.T. Rado and H. Suhl, Vol. III (Academic Press, New York, 1963) Ch. 4, p. 149; (b) Ann. Phys. 9 (1975) 93.
[9] V.A. Koptzik, Shubnikov Groups (Moscow University, Moscow, 1966).
[10] W. Opechowski and R. Guccione, in: Magnetism IIA, Eds. G.T. Rado and H. Suhl (Academic Press, London, 1965) ch. 3, p. 105.
[11] The authors wish to thank the referee for having brought this point to their attention.